Pressure-induced Magnetic Behaviors in $Ca_2Mn_2O_5$-type $A_2B_2O_5$ Perovskite-derived Structures

Yongjin Shin and James M. Rondinelli*
Department of Materials Science and Engineering, Northwestern University, Evanston, IL 60208, USA

We use density functional theory calculations to show the magnetic transition in $Sr_2Fe_2O_5$ (d^5) within $Ca_2Mn_2O_5$-type oxygen-deficient perovskites under applied hydrostatic pressure. The presence of ordered oxygen-vacancies in perovskites governs magnetic stability via changes in crystal field splitting with different anion geometry, polyhedral arrangement, and electronic configuration on transition metals. $Ca_2Mn_2O_5$-type structure is composed of square pyramidal units, whose crystal field splitting and connectivities yield different ground state magnetic order depending on the d-orbital electronic configuration; E-type antiferromagnetism (AFM-E) for $Sr_2Mn_2O_5$ (d^4) and AFM-G for $Sr_2Fe_2O_5$ (d^5). We continue to demonstrate that hydrostatic pressure reinforce the magnitude of crystal field spliting and affects magnetic stability which is also sensitive to electronic configuration. Specifically, we report that AFM-E order of $Sr_2Mn_2O_5$ is robust over applied pressure, whereas $Sr_2Fe_2O_5$ shows magnetic transition from AFM-G to ferromagnetism at ∼24.5 GPa with spin crossover. The effect of Hubbard U potential is also discussed that electronic correlation increases the electronic gap between spin up/down d-states, which addresses competitive correlation with external pressure for magnetic transition in $Sr_2Fe_2O_5$ as U works as a barrier for spin crossover. Finally, we evaluate the pressure effect induced by biaxial strain in vacancy ordered structures. With applied anisotropic stress with biaxial strain, it turns out to have pressure effect equivalent to 5 GPa.

I. INTRODUCTION

Magnetism in transition metal oxide (TMO) is of special interest as it is essential to interesting phenomena including colossal magnetoresistance (CMR), which is promising mechanism for next-generation memory devices. Those magnetic phenomena are originated from sensitive change in magnetic stability upon materials aspects including local coordination environment, polyhedral arrangement, and electronic configuration and local bond character. For example, $LaMnO_3$ has A-type antiferromagnetic (AFM-A)[1] order as ground state stabilized by Jahn-Teller distorted octahedra and their checker-board arrangement, but the other type of orders such as AFM-C, ferromagnetic (FM), and AFM-G can be stabilized depending on doping concentration in $La_{1-x}Sr_xMnO_3$.[2] Applying pressure such as hydrostatic pressure, biaxial strain, and chemical pressure, provides additional route to tune those stability, as the change in local bond character can affect the driving force to stabilize a certain magnetic order.[3]

Crystal field splitting (Δ_{CF}) originated from anion coordination environment changes the relative energy states of d-orbitals, and this change sensitively affects the magnetic interactions. Thus it is certain that presence of ordered oxygen-vacancies (OOV) modifies the Δ_{CF} with greater degree of change compared to the change induced by distortive atomic displacements. However, most endeavor of research on magnetic stability has been heavily focused on pristine perovskites, regarding the presence of vacancy as a type of point defect which does not disrupt bulk order although vacancy significantly reconstructs the local electronic structure of d-orbital by changing coordination environment. As external stimuli such as electric-field can drive phase transformation to OOV structures and tune electronic/ionic/optical/magnetic properties,[4] understanding magnetic bahavior with the presence of OOV will bring unparalleled benefits to materials engineering.

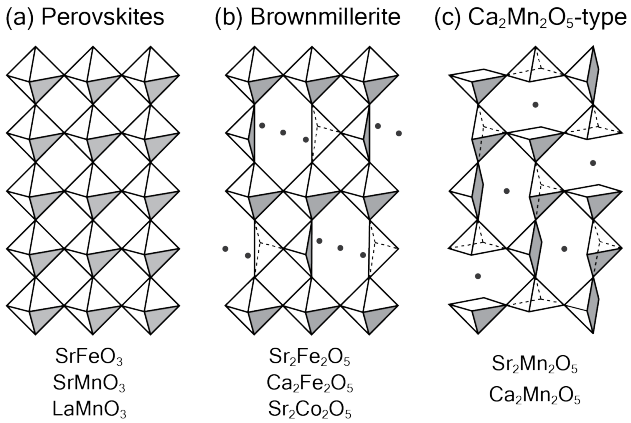

FIG. 1. Schematic illustration of (a) ABO_3 perovskites, (b) Brownmillerite, and (c) $Ca_2Mn_2O_5$-type structures based on polyhedral connectivities. Vacancies are drawn as gray dots, and prototypical compounds are listed below each structures.

In $A_2B_2O_5\square_1$ chemistry, there is one vacancy (□) per two ABO_3 perovskite units, which acts as if participating in stoichiometry. This $A_2B_2O_5$ chemistry adopts various polymorphs including phases illustrated in Fig. 1. Fig. 1(b) depicts brownmillerite structure where vacancies are formed along $[110]_p$ direction from pristine perovskites [Fig. 1(a)]. In result brownmillerite is made of alternative stacking of octahedral/tetrahedral layers, which is robustly adopted by $Sr_2Fe_2O_5$,[5,6] $Ca_2Fe_2O_5$,[7] $La_{2-x}A_xMn_2O_5$ (A=Ca, Sr, Ba),[8] and $Sr_2Co_2O_5$.[4] On the other hand, $Ca_2Mn_2O_5$-type in Fig. 1(c) has vacancies formed along $[001]_p$ direction, which in result composes

square pyramidal network with various connecting orientations. This structure type is adopted by $Ca_2Mn_2O_5$, $Sr_2Mn_2O_5$[9–11] or $Sr_2Fe_2O_5$ at high pressure.[12]

In this work, we report the relative stability in $Ca_2Mn_2O_5$-type structure as a result of complicated interplay between d-orbital configuration, external pressure, and crystal field splitting by utilizing density functional theory (DFT) calculations. We explain the ground state magnetic order of $Sr_2Mn_2O_5$ and $Sr_2Fe_2O_5$ at ambient pressure, which is consistent with Goodenough-Kanamori-Anderson (GKA) rule;[13–15] E-type antiferromagnetism (AFM-E) for $Sr_2Mn_2O_5$ and AFM-G for $Sr_2Fe_2O_5$. We further demonstrate the origin of magnetic behavior under hydrostatic pressure originated from reduced B-O bonds; it strengthens super-exchange interaction and further stabilizes AFM-E order in $Sr_2Mn_2O_5$ (d^4) while it assists spin crossover in $Sr_2Fe_2O_5$ (d^5) and drives AFM-G to ferromagnetism (FM) with simultaneous insulator-to-metal transition at ∼24.5 GPa. In line with this explanation the effect of electronic correlation is also covered by applying Hubbard U potential, where split of spin up/down states of d-orbitals is proven to overestimate the stability of FM in $Sr_2Mn_2O_5$ and suppress the spin crossover in $Sr_2Fe_2O_5$. Lastly we also estimate the pressure effect induced by biaxial strain, where its power is equivalent to 5 GPa quantified via measure of mangetic stabilities of $Sr_2Fe_2O_5$.

II. COMPUTATIONAL METHODS AND MATERIALS

We performed DFT calculations using the Vienna Ab-initio Simulations Package (VASP)[16,17] with the Perdew-Burke-Ernzerhof functional (PBE),[18] with the plus Hubbard U correction.[19] Projector-augmented wave (PAW) potentials[20] were used to describe the electron core-valence interactions with the following configurations: La($4f^0 5s^2 5p^6 5d^1 6s^2$) Sr ($4s^2 4p^6 5s^2$), Mn ($3d^6 4s^1$), Fe ($3d^7 4s^1$), and O ($2s^2 2p^4$). A 850 eV planewave cutoff is used to obtain the ground structures for each structure with 8×4×6 Monkhorst-Pack k-point mesh[21] for relaxation and self-consistent total energy calculations. Brillouin zone integrations employed the tetrahedron method.[22] The cell volume and atomic positions were evolved until the forces on each atom were less than 3 meV Å^{-1}. For the calculations involving Hubbard U potentials,[23] U=3 and 5 eV are initially applied to Mn and Fe atoms, and otherwise described in main text for discussion of correlation between U and external pressure. To evaluate the relative stabilities among different magnetic orders, enthalpies H=E+PV are calculated where external pressure was applied by adding Pulay correction to the stress tensor with 10 GPa intervals. Exchange coupling (J) constants are calculated as an effective parameters so that $\hat{S}_i$ and $\hat{S}_i$ in Heisenberg's model $H = \sum_{i,j} J_{ij} \hat{S}_i \hat{S}_j$ become unit vectors.[?] The coupling constants are calculated by applying different magnetic orders on structures

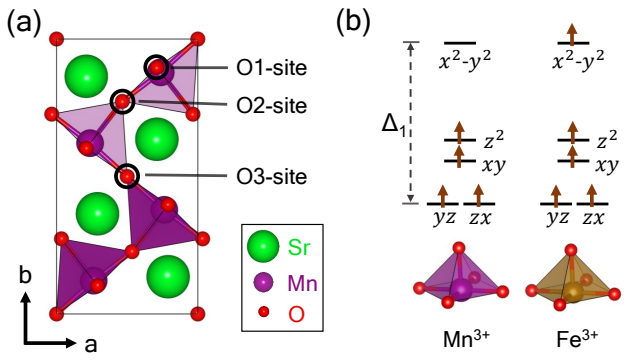

FIG. 2. (a) Atomic structure of $Ca_2Mn_2O_5$-type structure. AFM-E order is indicated by thickness of colors; up-spin (thick) and down-spin (thin) (b) d-orbital filling for Mn^{3+} and Fe^{3+} ions in BO_5 square pyramidal coordination environment.

of the most stable magnetic order at each pressure. We induced antiferromagnetic or ferromagnetic interaction on each type of bridging oxygens, which yields 8 different magnetic orders from 3 types of oxygen sites (2^3=8).

Fig. 2(a) describes the atomic structures of $Sr_2Mn_2O_5$ which has $Pbam$ symmetry. This $Ca_2Mn_2O_5$-type structure consists of BO_5 square pyramidal units, where three different O-sites bridge the pyramids in different ways. The O1 and O3 sites correspond to the basal positions for both neighboring pyramids along c-axis and on ab-plane, respectively, whereas the O2-site corresponds to the apical oxygen that bridges the BO_5 vertex of one unit to the basal oxygen of another. The square pyramidal crystal field resembles that of Jahn-Teller distorted octahedral crystal field splitting in $LaMnO_3$. The orbital states associated with z character are lowered owing to the absence of one oxygen along z (apical) direction, and e_g and t_{2g} states are further split. This feature is related to longer apical Mn-O bond than basal bonds, to minimize the electrostatic instability with d electrons when d^4 configuration of Mn^{3+} fills up to d_{z^2} and leaves $d_{x^2-y^2}$ empty. This $Ca_2Mn_2O_5$-type structure is also adopted by $Sr_2Fe_2O_5$ by having reconstructive phase transition from brownmillerite under high pressure,[12,24] which makes this phase an appropriate sample structure to investigate the effect d-orbital filling with ordered oxygen vacancies.

III. RESULTS AND DISCUSSION

A. Magnetic Stability at Ambient Condition

$Ca_2Mn_2O_5$-type structure can host an AFM-E magnetic order via super-exchange interaction when square pyramidal crystal field, polyhedral arrangement, and d^4 electronic configration are combined as depicted in Fig. 2.[3,25] As transition metal with d^4 configuration has half-filled d-orbitals except for $d_{x^2-y^2}$, the magnetic interaction between pyramids is determined by their connectiv-

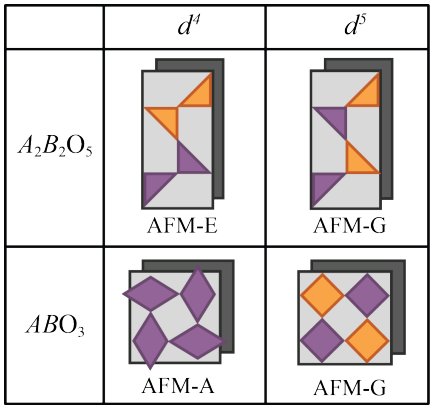

FIG. 3. Schematic illustration of ground state magnetic orders with varying polyhedral unit and d-electronic configuration. Magnetic orders are indicated based on color; purple and orange polyhedra up and down spin, respectively, and dark grey plane is used for inter planar antiferromagnetic interaction.

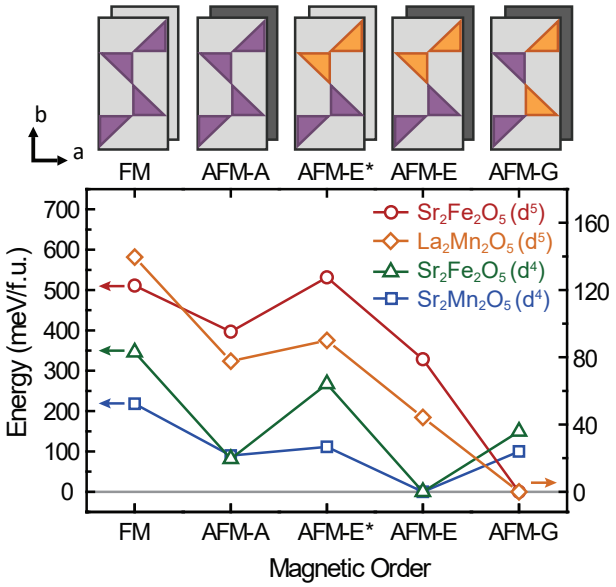

FIG. 4. Energy landscape of different magnetic orders in $A_2B_2O_5$ compounds with square pyramidal network oabtained at DFT-PBE level with U of 3 and 5 eV are applied to Mn and Fe, respectively. Magnetic orders are indicated based on color; each purple and orange polyhedra up and down spin, respectively, and dark grey plane is used for antiferromagnetic interaction between atomic layers along c-direction.

ities: O1 and O3 connection becomes antiferromagnetic owing to interaction between empty orbitals, and O2 connection ferromagnetic because of the imaginary hopping between empty and half-filled orbitals.

Though Jahn-Teller distorted perovskites share similar d-orbital levels with square pyramidal crystal field splitting, the difference in polyhedral arrangement changes the resultant magnetic orders as illustrated in Fig. 3. In down-left cell of Fig. 3, there are two orientation of elongated octahedra and they form checker-board arrangement on $(001)_p$-plane. Thus on one $(001)_p$-plane, all connections between square pyramids becomes ferromagnetic interactions via super-exchange interpretation of GKA-rule. On the other hand, connections along $[001]_p$ direction addresses overlap of empty $d_{x^2-y^2}$ orbitals and makes antiferromagnetic interplanar interaction.[1]

It is noteworthy that AFM-E order in $Sr_2Mn_2O_5$ is stabilized by conventional A-cation, which contrasts to RMnO$_3$ perovskites in that its AFM-E order is only stabilized by insertion of rare earth element to induce higher degree of lattice distortion and activate the magnetic interaction from second-nearest neighbors.[26] In $Sr_2Mn_2O_5$, on the other hand, square pyramidal crystal field splitting owing to ordered oxygen-vacancies stabilizes the AFM-E order. The relative stability of AFM-E order in $Sr_2Mn_2O_5$ and RMnO$_3$ can be deduced from Néel temperature T$_N$. $Sr_2Mn_2O_5$ has T$_N$ of 380 K, which contrasts to RMnO$_3$ has less than T$_N$ <50 K.[27–29]

The ground state magnetic order in $A_2B_2O_5$ can be altered by orbital filling. $Sr_2Fe_2O_5$ is an appropriate example of this case as it adopts the square pyramidal network under high perssure,[12] while Fe^{3+} with d^5 configuration makes all d-orbitals half-filled. As this orbital configuration inhibit electron hopping of same spin direction between orbitals, every Fe-O-Fe bond forms antiferromagnetic interaction. This behavior stabilizes AFM-G order regardless of polyhedral connectivities in corner-connected network. In the right column of Fig. 3, the checkerboard-like ordering is illustrated in both $A_2B_2O_5$ and perovskites structures.

TABLE I. Bond length of square pyramid in $Sr_2Mn_2O_5$, $Sr_2Fe_2O_5$, and $La_2Mn_2O_5$ at ambient pressure (0 GPa). Apical bond (l_{ap}), and average basal bonds ($l_{ba,ave}$) follow the unit of Å, while unit cell volume the unit of Å^3.

System	d-filling	Order	l_{ap}	$l_{ba,ave}$	$l_{ap}/l_{ba,ave}$
$Sr_2Fe_2O_5$	d^5	AFM-G	1.89	1.98	0.97
$La_2Mn_2O_5$	d^5	AFM-G	2.04	2.14	0.96
h-$Sr_2Fe_2O_5$	d^4	AFM-E	1.84	1.81	1.02
$Sr_2Mn_2O_5$	d^4	AFM-E	2.09	1.94	1.08

To confirm the validity of GKA-rule on predicting ground state magnetic order in $Ca_2Mn_2O_5$-type structures, we plotted energy landscape for $Sr_2Mn_2O_5$, $Sr_2Fe_2O_5$, and $La_2Mn_2O_5$ with different magnetic orders in Fig. 4 by performing DFT-PBE calculations. As expected, AFM-E and AFM-G order are the most stable for $Sr_2Mn_2O_5$, and $Sr_2Fe_2O_5$, respectively, which means super-exchange interaction provides appropriate intuition on magnetic stability at ambient condition. The both AFM order in two compounds are insulators where band gap formed by different orbital characters. In $Sr_2Mn_2O_5$, d^4 configuration half-fills d-orbital up to d_{z^2} and the band gap is formed with conduction band of $d_{x^2-y^2}$. In $Sr_2Fe_2O_5$, on the other hand, all d-states are half-filled then conduction band is composed with spin down d-orbitals and the electron hopping between Fe sites are

prohibited by Hund's rule. To better capture the role of d-electron filling, we tested for hole-doped $Sr_2Fe_2O_5$ (h-$Sr_2Fe_2O_5$) with nominal d^4 configuration and $La_2Mn_2O_5$ (d^5).

La is well known for element compatible with $Sr_2Mn_2O_5$ chemistry which dope electron to Mn atoms.[2,8,30,31] Thus we performed calculations for $La_2Mn_2O_5$, which yields nominally d^5 configuration with manganese.[32] The general shape of energy landscape was intact regardless of Hubbard U potential in $Sr_2Fe_2O_5$ and $Sr_2Mn_2O_5$. As plotted in Fig. 4, energy landscapes can be categorized by compounds' d-electron configurations regardless of B-cation element, which means that d-orbital filling has deterministic effect on ground state magnetic order at ambient condition.

Local bonding character within individual polyhedron is another feature significantly affected by d-configuration. Specifically, the bond ratio $l_{ap}/l_{ba,ave}$ is highly dependent on d-orbital filling because d^4 $Sr_2Mn_2O_5$ and h-$Sr_2Fe_2O_5$ are with elongated polyhedra along apical direction while $Sr_2Fe_2O_5$ and $La_2Mn_2O_5$ with d^5 are not (Table I). This feature in $Ca_2Mn_2O_5$-type structure can be understood in the same context with Jahn-Teller distortion in ABO_3 perovskites. $LaMnO_3$ is d^4 Jahn-Teller active system therefore has elongated octahedron to stabilize the system by removing the degeneracy in e_g orbital. On the contrary, d^5 systems for instance $LaFeO_3$ and $SrMnO_3$ do not have such elongated octahera,[33,34] as illustrated in Fig. 3. Likewise, as $Ca_2Mn_2O_5$-type structure has similar crystal field splitting with Jahn-Teller distorted octahedra, $Sr_2Mn_2O_5$ can be stabilized by having longer l_{ap} than $l_{ba,ave}$ while d^5 systems have no energetic merit of having distorted bonding environment.

B. Pressure-dependent super-exchange interaction in $Sr_2Mn_2O_5$

When hydrostatic pressure is applied, relative stabilites among mangnetic orders in $Sr_2Mn_2O_5$ change, where AFM-E order becomes more stable compared to other magnetic orders. As shown in Fig. 5(a), FM order has 200 meV higher enthalpy per formula unit than AFM-E order at 0 GPa, and it increases to 700 meV when 30 GPa is applied. Other AFM orders (A, E*, and G), on the other hand, are unstable by ~100 meV/f.u. at 0 GPa, but their enthalpies increase by different degrees: AFM-A to 387 meV, AFM-E* to 246 meV, and AFM-G to 95 meV at 30 GPa.

To understand the different evolution of instabilites for magnetic orders under pressure, we calculated exchange coupling constants between Mn atoms as plotted in Fig. 5(b). J_1, J_2 and J_3 represent the coupling via O1, O2, and O3 connections, respectively, and they show clear contrast especially under high pressure. Calculated J_1 and J_3 are positive values while J_2 is negative, which supports the AFM-E order with the lowest energy. Based on Heisenberg's model, $H = \sum_{i,j} J_{ij}\hat{S}_i\hat{S}_j$, the ground

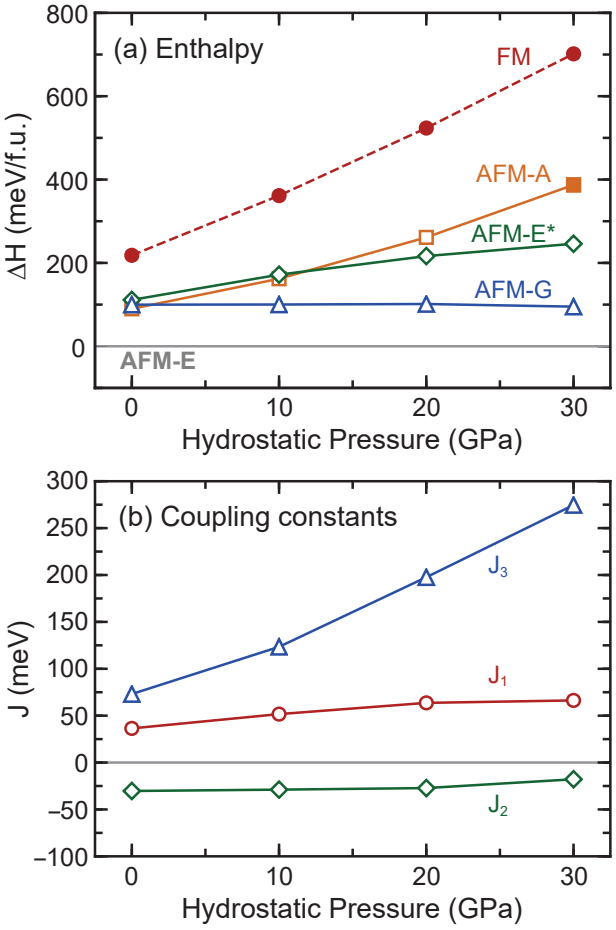

FIG. 5. (a) DFT-PBE level relative enthalpy differences of different magnetic orders with respect to AFM-E order in $Sr_2Mn_2O_5$ under hydrostatic pressure. No Hubbard potential is applied (U=0 eV), and metallic phases are drawn with filled symbol connected with dashed line. (b) The exchange coupling constants between Mn atoms, where J_1, J_2 and J_3 correspond to O1, O2, and O3 connections, respectively.

state magnetic order can be achieved by antiferromagnetic connection on O1 and O3 connections with positive J constants while ferromangetic interaction on O2 for negative J. This formulation also explains the origin of instabilities for other magnetic orders: each AFM-E*, AFM-G, and AFM-A order gains instability from J_1, J_2, and J_3, respectively, by deviating optimum magnetic order (AFM-E), while FM gain from both J_1 and J_3.

The pressure-dependent relative stabilities are also closely associated with J constants. J_1 and J_3 significantly increase from 36 and 72 meV to 66 and 274 meV at 30 GPa, respectively, while J_2 barely changes upon hydrostatic pressure. In result, magnetic orders gain varying degree of instabilities depending on their magnetic interactions different from AFM-E order and corresponding J constants. Note that the number of O3 connections are half of O1 or O2 connections, then this analyis based on Heisenberg's model recovers the pressure-dependent stabilities in Fig. 5(a). Instability of AFM-A is higher

than that of AFM-E* at high pressure, because their instabilities are originated from J_3 and J_1, respectively. FM spontaneously gains highest instabiliy by having both energetic demerit from both J_1 and J_3, and AFM-G order maintain similar level of instability. Reinforcement in super-exchange interaction is general behavior because the bond length B-O decreases.[36–38] Thus the increasing instability in Fig. 5(a) can be attributed to pressure decreasing general bond length, while the detailed trend depends on polyhedral connections.

The relationship between bond length and superexchange interaction provide intuition about different unit volume of $Sr_2Mn_2O_5$ depending on magnetic orders. Hydrostatic pressure generally drives the materials system toward smaller unit volume, which accompanies shorter bond length and reinforced super-exchange interaction. This trend further stabilizes the AFM-E order, while the energetic cost for other magnetic orders becomes larger especially when they are associated with J_1 and J_3. Thus non-ground state magnetic orders are relaxed with relatively longer bond length so as to reduce the energetic cost. Indeed, AFM-A, -E*, and FM order are with larger unit volume compared to AFM-E order, while AFM-G order shows similar value to AFM-E (Table II and supplementary information).

TABLE II. Unit cell volume and bond length of square pyramid in $Sr_2Mn_2O_5$ with different pressure (P). Apical bond (l_{ap}), and average basal bonds ($l_{ba,ave}$) follow the unit of Å, while unit cell volume the unit of Å^3.

Order	Pressure	Volume	l_{ap}	$l_{ba,ave}$	$l_{ap}/l_{ba,ave}$
AFM-E	0	455	2.07	1.92	1.08
	10	421	2.04	1.89	1.08
	20	394	2.03	1.87	1.09
	30	374	2.03	1.85	1.10
AFM-G	0	455	2.07	1.92	1.08
	10	421	2.03	1.89	1.08
	20	394	2.03	1.86	1.09
	30	374	2.03	1.85	1.10
FM	0	464	2.02	1.94	1.04
	10	431	1.99	1.91	1.04
	20	405	1.97	1.88	1.05
	30	385	1.95	1.87	1.04

It is noteworthy that pressure-dependence shows anisotropy regarding J_2 interaction and its consequential instability of AFM-G order, which is generally insensitive to hydrostatic pressure. This implies that the magnetic interaction of O2 site connection, where $d_{x^2-y^2}$ and d_{z^2} are associated for double-exchange interaction, are insensitive to pressure. Super-exchange is reported as able to dominate double-exchange interaction under compressive condition,[39,40] meaning double-exchange interaction is relatively insensitive to pressure compared to super-exchange. Thus small change in J_2 constant and its consequent instability of AFM-G order with respect to pressure can be understood from its distinction

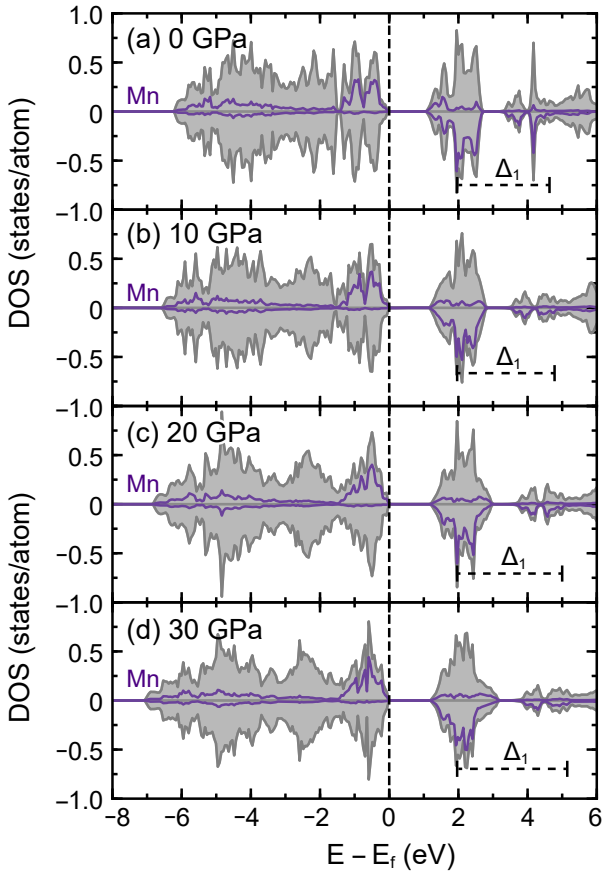

FIG. 6. Electronic density of states of $Sr_2Mn_2O_5$ with AFM-E order under pressure of (a) 0 GPa, (b) 10 GPa, (c) 20 GPa, and (d) 30 GPa.

from O1 and O3 connections in d^4 $Ca_2Mn_2O_5$-type structure. Another interpretation can partially made from the anisotropic contraction in bond length (Table II). In AFM-E order, l_{ap} decreases by 2 % compared to twice larger change in $l_{ba,ave}$ of 4 %. This means apical bond is relatively stiffer than basal bonds, and interaction via O2 connection occurs relatively constant distance under pressure.

Since there is no change of sign in J constants under hydrostatic pressure, GKA-rule predicting magnetic stabilities is still valid and the discussion can be reduced to the crystal field splitting. As hydrostatic pressure induces compressive condition for materials and reduces the general bond length, the crystal field splitting via anionic coordination is also reinforced. This effect can be roughly quantified from density of states (DOS), as plotted in Fig. 6. On the conduction band spin-down DOS of one Mn atom is plotted with purple color resembles the square pyramidal crystal field splitting decribed in Fig. 2(b). To capture the Δ_1, we measured the energy difference of the DOS peaks in purple color as annotated. The measured value increases with respect to pressure, from 2.73 at 0 GPa to 2.82, 3.04 and to 3.18 at 30 GPa. Thus the

enhanced relative stability of AFM-E order is also shown from electronic structure, by rough measure of crystal field splitting and its impact on magnetic stabilities.

The stable AFM-E order in $Sr_2Mn_2O_5$ under pressure is distinct from AFM order of other d^4 manganites in pristine ABO_3 perovskites. AFM-A order of $LaMnO_3$ becomes unstable under pressure as Jahn-Teller distortion is suppressed under hydrostatic pressure, and eventually exhibit insulator-to-metal transition.[41–43] In $RMnO_3$, stability of AFM orders depend on the selection of R element and the role of f-orbital. While AFM-A order which competes with AFM-E in $EuMnO_3$ shows magnetic transition toward FM order at ∼2 GPa,[44] $YMnO_3$ shows reinforced stability of AFM-E order[45] but it is known that AFM-E order in $YMnO_3$ is with very low T_N and synthesizable with limited condition.[46,47] Considering the distinction of $Sr_2Mn_2O_5$ in $Ca_2Mn_2O_5$-type structure with other d^4 manganites, we can conclude that crystal field splitting of square pyramidal network and the arrangement of the pyramids provides a tuning opportunity of a certain magnetic order.

C. Pressure-dependent Magnetic Transition in $Sr_2Fe_2O_5$

To evaluate the relative magnetic phase stabilities of $Sr_2Fe_2O_5$ with d^5 configuration under different external pressure, we plotted enthalpy and exchange coupling constants of structures in Fig. 7(a) at the DFT-PBE level (U=0). The most noticeable pressure-dependent change is that the relative enthalpies of magnetic orders to AFM-G order decrease with respect to pressure, which is opposite to the magnetic behavior in $Sr_2Mn_2O_5$. At the end of the trend magnetic transition from AFM-G to FM is derived by hydrostatic pressure at ∼24.5 GPa. As FM phase is metallic, this AFM-G to FM magnetic transition accompanies insulator-to-metal transition. Metallicity was also found from magnetic orders other than AFM-G at high pressure. AFM-E as another exception showed insulating behavior at 0 GPa but becomes metal over 10 GPa, and its relative stability starts to decrease compared to AFM-G like other metallic orders.

Exchange coupling constants in Fig. 7(b) are consistent with this magnetic transition that all constants decrease from positive value and becomes negative at higher pressure. Thus any magnetic interaction between opposite spins leads to energetic cost based on Heisenberg formulation. Similar to the earlier section, the energy difference between FM and AFM-G order can be interpreted by summed J_1, J_2, and J_3. Considering that J_1 and J_2 curves are with the steep slope compared to J_3, we can conclude that the magnetic transition is mainly drived by J_1 and J_2 via O1 and O2 connections in the structure. This magnetic transition in $Sr_2Fe_2O_5$ is an unique behavior when compared to $Sr_2Mn_2O_5$ in that AFM-G order in $Sr_2Fe_2O_5$ is also stabilized by super-exchange interactions like $Sr_2Mn_2O_5$, but its stability is rather

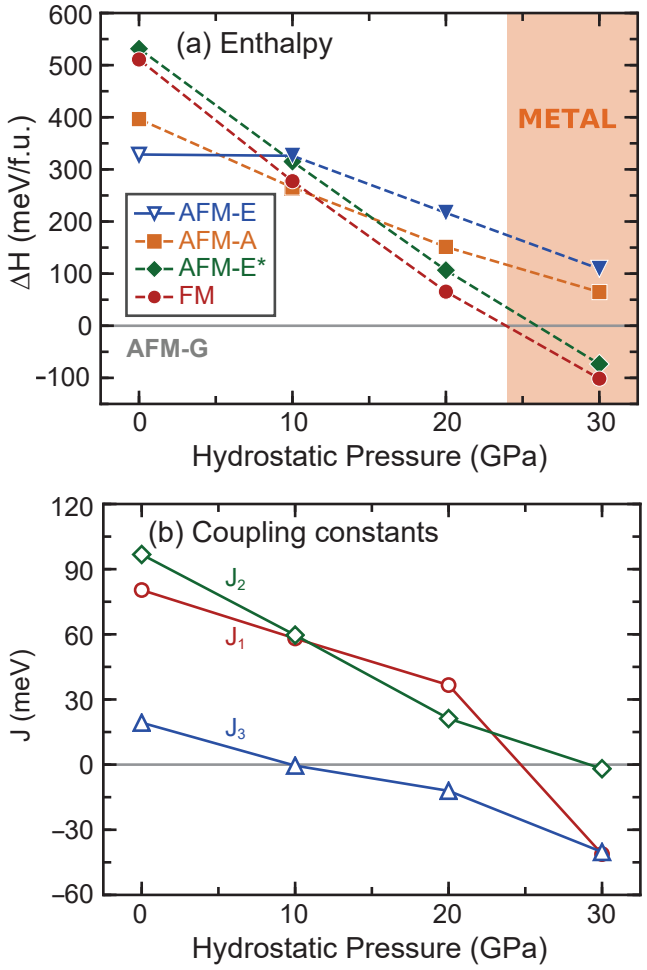

FIG. 7. (a) DFT-PBE level relative enthalpy differences of different magnetic orders with respect to AFM-E order in $Sr_2Mn_2O_5$ under hydrostatic pressure. No Hubbard potential is applied (U=0 eV), and metallic phases are drawn with filled symbol connected with dashed line. (b) The exchange coupling constants between Fe atoms, where J_1, J_2 and J_3 correspond to O1, O2, and O3 connections, respectively.

weakened under pressure opposite to the AFM-E order in $Sr_2Mn_2O_5$. This difference implies that a mechanism other than super-exchange is the origin of the transition.

Density of states (DOS) of $Sr_2Fe_2O_5$ in Fig. 8 reveal that the magnetic transition accompaning insulator-to-metal transition is derived from high-spin to low-spin transition on Fe atoms. Projected DOS of one Fe atom, especially with AFM-G order, well describes the square pyramidal crystal field splitting of d-orbital depicted in Fig. 2(b) and so forth the width of the splitting defined by Δ_1. This projected DOS clearly shows that AFM-G order is insulating because d^5 configuration only filling the spin-up states of d-orbital. On the other hand, in FM order the up/down states overlap each other by some fraction, which makes the $Sr_2Fe_2O_5$ metallic. Note that here the electron hopping would occur via minority spin, so the conductivity of the metal would be not be sufficiently high. Magnetic moments on Fe atoms also corroborate the spin crossover.

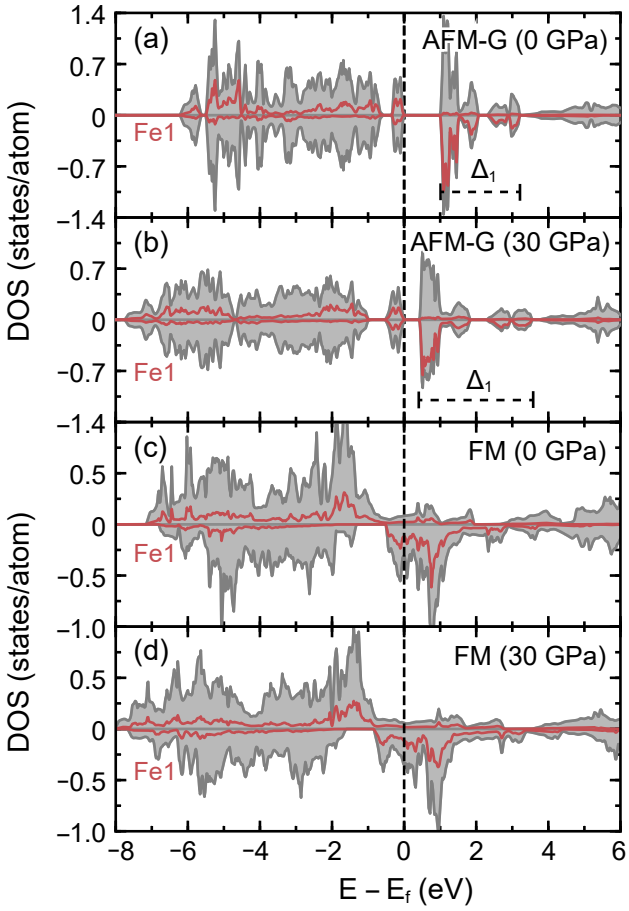

FIG. 8. Electronic density of states of $Sr_2Fe_2O_5$ with different mangetic orders and pressures without Hubbard potential. (a) AFM-G at 0 GPa, (b) AFM-G at 30 GPa, (c) FM at 0 GPa, and (d) FM at 30 GPa.

The moment is 3.49 μ_B in AFM-G phase at 0 GPa, but it decreases down to 2.67 μ_B in FM phase under 30 GPa, meaning spin character of some electrons are screened by opposite-spin electrons in FM under high pressure. This means pressure-induced magnetic transition from AFM-G to FM involves spin crossover, making some spin-up electrons at higher energy level transit to spin-down states.

The energetic motive of spin crossover can be found from band widening effect by hydrostatic pressure on d-orbital. In Fig. 8, states are broadened upon hydrostatic pressure in both magnetic orders. The broadening in valence band can be attributed to enhanced hybridization between Fe-d and O-p orbital owing to higher orbital overlap with shorter M-O bond length. Indeed, the average Fe-O bond length decreases from 1.96 Åto 1.88 Åin AFM-G order, and 1.94 Åto 1.87 Åin FM at 0 GPa and 30 GPa, respectively. The conduction band is also subject to widening, but its origin can be interpreted as reinforced crystal field splitting effect as discussed in earlier section. Especially in AFM-G order of $Sr_2Fe_2O_5$, the d-orbital in conduction band is isolated from other states whose definitive edge enables the quantitative comparison of crystal field splitting (Δ_1). The Δ_1 increases by 0.92 eV with 30 GPa of hydrostatic pressure, from 2.29 eV at 0 GPa to 3.21 eV at 30 GPa. This band broadening via reinforced crystal field splitting reduces the the band gap (E_g) in AFM-G order, from 0.85 eV to 0.2 eV, which lowers the energetic barrier spin crossover for FM order between occupied d-states (spin-up electrons of Fe) and unoccupied states (spin-down).

The presence of spin crossover induces the dictinction of unit volume in $Sr_2Fe_2O_5$ when compared to $Sr_2Mn_2O_5$ that GKA-predicted AFM-G ground state order is not with the smallest unit volume. Unlike $Sr_2Mn_2O_5$ having larger unit volume when a magnetic order more deviates from ground state magnetic roder, FM order in $Sr_2Fe_2O_5$ has smaller volume than AFM-G as shown in Table III. Indeed, FM order has the smallest unit volume. As ions have smaller radii with low-spin configuration compared to high-spin,[48] Fe^{3+} obtains smaller radii in FM order than in AFM-G order, making smaller unit volume with spin crossover occurs. Calculation on AFM-E order clearly shows this effect because its unit volume is larger than that of AFM-G at 0 GPa but becomes smaller above 10 GPa. This is also the point that AFM-E order becomes metallic via spin crossover, showing that spin crossover is the key determining the unit volume.

TABLE III. Unit cell volume and bond length of square pyramid in $Sr_2Fe_2O_5$ with different pressure (P). Apical bond (l_{ap}), and average basal bonds ($l_{ba,ave}$) follow the unit of Å, while unit cell volume the unit of Å^3.

Order	Pressure	Volume	l_{ap}	$l_{ba,ave}$	$l_{ap}/l_{ba,ave}$
AFM-G	0	468	1.90	1.97	0.96
	10	432	1.89	1.93	0.98
	20	405	1.91	1.89	1.00
	30	383	1.90	1.87	1.02
AFM-E	0	473	1.90	1.99	0.96
	10	425	1.92	1.91	1.01
	20	398	1.91	1.87	1.02
	30	377	1.91	1.87	1.03
FM	0	453	2.01	1.92	1.05
	10	418	2.01	1.91	1.07
	20	393	2.00	1.89	1.08
	30	374	1.99	1.87	1.08

Together with unit volume, the bond length ratio $l_{ap}/l_{ba,ave}$ also senstively reacts to spin crossover. In Table III, $l_{ap}/l_{ba,ave}$ changes from 0.96 to 1.02 in AFM-G by pressure, but FM has range of 1.05-1.08 which is closer to the range of $Sr_2Mn_2O_5$. In addition, as l_{ap} of AFM-E order also becomes longer than $l_{ba,ave}$ at 10 GPa, this higher bond length ratio can be regarded as a sign of spin crossover in $Sr_2Fe_2O_5$. As spin crossover occurs electron in up-spin $d_{x^2-y^2}$ state transit to lower spin-down d-states, where empty $d_{x^2-y^2}$ leads to the similar structural feature with d^4 system. The change in the

$l_{ap}/l_{ba,ave}$ ratio is mainly drived by the $l_{ba,ave}$, in that l_{ap} barely changes either by pressure or spin crossover. This behavior again can be understood as an endeavor to minimize the energetic cost of hosting electron in d_{z^2} orbital by maintaining longer l_{ap} bond. This structural difference is closely related to magnetic interaction as seen from Fig. 7(b). The trend abruptly changes at 20 GPa, especially for J_1, because the FM structure is used for exchange coupling constants as ground state structure on that pressure. Indeed, when AFM-G structure relaxed at 30 GPa is used for calculation, we found that the linear trend is maintained up to 30 GPa. Thus we can deduce that the difference in $l_{ap}/l_{ba,ave}$ between AFM-G and FM is responsible for this anisotropic change.

Summarizing the effect of hydrostatic pressure in $Sr_2Fe_2O_5$ with d^5 configuration, band broadening in unoccupied d-states in conduction band assists spin crossover and stabilizes the ferromagnetic interactions. This behavior can be attributed to the d^5 configuration as in $Sr_2Mn_2O_5$ the band broadening in d-orbital would increases the band gap composed by spin-up d_{z^2} and $d_{x^2-y^2}$ states, which further inhibits the electron hopping.[35] Indeed, we found that pressure works favorable toward FM order is universal in other d^5 systems. $Ca_2Fe_2O_5$ showed transition at ∼17 GPa, and FM order in $La_2Mn_2O_5$ becomes further stabilized with pressure.(Suppl to be included) Thus it is easily deducible that this magnetic transition with increased crystal field splitting can also occur in other elements when appropriate d-orbital configuration is provided. In addition, other types of polyhedral unit such as octahedron and square plane can host spin crossover via band broadening effect with different critical pressure. Indeed, transitions with spin crossover are commonly oberved in other types of ferrite compounds with comparable pressure range: $SrFeO_2$ (square planar) at 33 GPa,[50,51] $CaFeO_3$ at ∼30 GPa,[52] and $BiFeO_3$ at ∼40 GPa.[53]

At ambient pressure, $Sr_2Fe_2O_5$ is known to exhibit structural transition from brownmillerite structure which consists of alternative stacking of octahedral and tetrahedral layers, to square pyramidal network at 19.7 GPa.[12,24] To the best of our knowledge, the magnetic structure of $Sr_2Fe_2O_5$ with *Pbam* symmetry at lower temperature has not been investigated while without cooling it exhibits paramagnetism.[12] Thus we predict FM phase for $Sr_2Fe_2O_5$ at high pressure with controlled low temperature, with metallicity derived from spin crossover.

D. Effect of Hubbard U potential

The both super-exchange and spin crossover are sensitive to relative orbital energies, so the effect of Hubbard U potential is expected to be non-trivial as it affects these behaviors by shifting occupied orbitals down and unoccupied up in the energy. Given electronic configurations in Fig. 2(b), we anticipate finite U value in Mn and Fe affects pressure-magnetic property relationship of $Sr_2Mn_2O_5$ and $Sr_2Fe_2O_5$ via tuning band gap (E_g), square pyramidal crystal field splitting (Δ_1), and average bond length (l_{ave}). In Fig. 9, we plotted the DFT-PBE level relative enthalpies with U potential of 3 eV and 5 eV are applied to Mn and Fe atoms, which follows the generally acceptable values.[12,44,54–56] As a result of U potential we confirmed that band gap increases for insulating structures and some metallic phases change to insulators while Δ_1 diminished as summarized in Table IV.

TABLE IV. Band gap (E_g), square pyramidal crystal field splitting (Δ_1), and average bond length (l_{ave}) in $Sr_2Mn_2O_5$ and $Sr_2Fe_2O_5$ depending on applied U potential value. The structures are with ground state magnetic orders (AFM-E for $Sr_2Mn_2O_5$, AFM-G for $Sr_2Fe_2O_5$) at ambient pressure.

Order	U	E_g	Δ_1	l_{ave}
$Sr_2Mn_2O_5$	0	1.09	2.73	1.95
	3	1.61	1.93	1.97
$Sr_2Fe_2O_5$	0	1.00	2.29	1.96
	2	1.90	1.74	1.97
	5	2.32	1.64	1.97

In $Sr_2Mn_2O_5$, AFM-E order is still the most stable over the whole pressure range as it is plotted in Fig. 9(a), and the pressure dependences stay same regardless of U potential: enthalpy of AFM-A, AFM-E*, and FM increases with pressure while AFM-G barely changes. The energy difference between AFM-G and -E slightly increases with on-site potential (U), from ΔE of ∼100 to ∼130 meV/f.u, which means that AFM-E order is more stabilized with respect to AFM-G order. On the other hand AFM-E*, AFM-A and FM orders are more stabilized by U, having more than ∼50% of reduction in energy difference with respect to AFM-E order, as can be seen in the change of scale in Fig. 9(a), compared to Fig. 5(a). Compiling these observations, the stabilization effect of U can be rewritten as a hierarchy of AFM-G < AFM-E < AFM-E* < AFM-A < FM, whose trend is maintained over entire pressure range. This hierarchy also roughly follows the sum of ferromagnetic interactions strength among square pyramidal units; as AFM-G (all antiferromagnetic), AFM-E (ferromagnetic J_2), AFM-E* (ferromagnetic J_2 and J_1), AFM-A (ferromagnetic J_2 and J_3), and FM (all ferromagnetic).[49] Thus we can deduce that on-site potential U has stabilizing effect on FM interactions, while the difference between AFM-E* and AFM-A despite the same number of ferromagnetic interactions can be attributed to the relatively subtle difference in bonding type O1 and O3. This trend is consistent with other studies which demonstrated LSDA+U formalism considered to overestimate the tendency toward ferromagntism in $LaMnO_3$ and $YMnO_3$.[26,57]

The on-site potential U on $Sr_2Fe_2O_5$ (d^5), in contrary, addresses the opposite pressure-dependent trend, which is distinct from that of $Sr_2Mn_2O_5$. The enthalpies of other magnetic orders increase with respect to AFM-G order, in result no magnetic transition from AFM-G to FM order

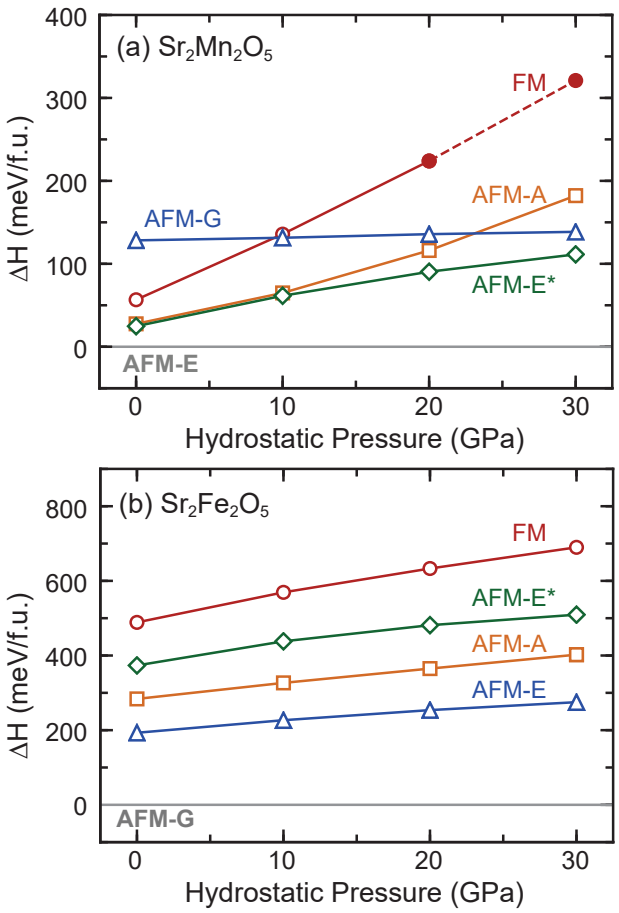

FIG. 9. DFT-PBE level relative enthalpy differences between different magnetic orders for (a)$Sr_2Mn_2O_5$ and (b)$Sr_2Fe_2O_5$ under hydrostatic pressure. Hubbard potential of 3 and 5 eV were applied to Mn and Fe, respectively. The reference energy was set to the ground state magnetic order of each compounds at ambient pressure.

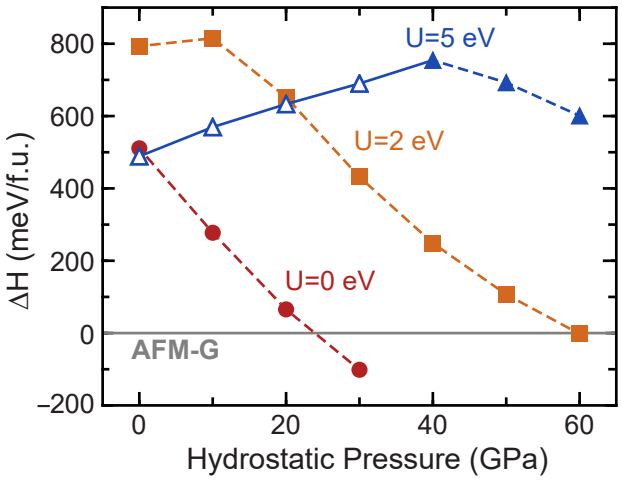

FIG. 10. Relative energy difference of FM $Sr_2Fe_2O_5$ phases compared to AFM-G phases with respect to hydrostatic pressure.

found within 0 to 30 GPa range. Indeed, the relative enthalpy of FM becomes the highest at high pressure, meaning FM phase changes from the most stable to the most unstable by the presence of U potential. In addition, all magnetic orders become insulator after U is applied as indicated by empty symbols in Fig. 9. Even FM order opens a band gap of 0.72 eV at 0 GPa and having high-spin d^5 configuration without occupied spin-down states of Fe. This absence of spin transition can be attributed to the general effect of U on transition metals. As d-orbital states are more localized, band gap increases and a barrier for spin crossover is addressed. Applied on-site potential changes the governing mechanism for pressure-dependent behavior in $Sr_2Fe_2O_5$ to super-exchange like in $Sr_2Mn_2O_5$, as spin crossover is suppressed by U.

As U activates the conventional super-exchange behavior, the pressure-dependent magnetic stabilities of $Sr_2Fe_2O_5$ can be also explained based on the degree of GKA-rule violation. This trend is almost precisely scalable by the number of ferromagnetic interaction of each magnetic orders in Fig. 9(b). There are eight O1-sites, eight O2-sites, and four O3-sites among total 20 connecting oxygens in one magnetic unit cell, which hosts J1, J2, and J3 coefficients. By scoring the violation of GKA-rule in each magnetic order, AFM-E is 8 (J_2), AFM-A is 12 (J_2, J_3), AFM-E* is 16 (J_1, J_2), and FM is 20 (J_1, J_2, J_3), which matches the nearly equally distanced enthalpy curves and doubly spaced distance between AFM-E and -G in Fig. 9(b). Indeed, the stability hierarchy between AFM-A and -E* in $Sr_2Fe_2O_5$ is reversed from that in $Sr_2Mn_2O_5$, where AFM-A showed higher instability than AFM-E* owing to distinctly strong J_3 constant. These two observations imply that every connection in d^5 $Ca_2Mn_2O_5$-type structure is comprised with magnetic connections of nearly same strength, when spin transition is suppresed and super-exchange is dominant.

To evaluate the supression of spin crossover with application of U in d^5 system, we plotted pressure-dependent magnetic stabilities between FM and AFM-G order of $Sr_2Fe_2O_5$ in Fig. 10 with additional calculation with applying U=2 eV under wider range of hydrostatic pressure up to 60 GPa. When the hydrostatic pressure range is extended, calculations with U=5 eV showed that the energy difference of FM with respect to AFM-G makes a peak at 40 GPa and starts to decrease after that point. As metallicity indicated as filled symbol in Fig. 10, FM phase becomes metallic at 40 GPa where spin crossover occurs simultaneously. The decrease in enthalpy relative to AFM-G order can be attributed to the enhanced spin crossover under pressure similar to when U is not applied. Calculations with U=2 eV shows similar relationships by having peak at 10 GPa, which is lower pressure than that of U=5 eV calculations. Eventually magnetic transition from AFM-G to FM order occurred at ~60 GPa, which accompanies insulator-to-metal transition and spin crossover. This relationship tells us that U hosts a barrier for spin crossover and activates the reinforcement of

antiferromagnetic interaction,[58] whch varies depending on U value, but such effect is surmountable with higher level of applied pressure.

E. Effect of Biaxial Strain on $Sr_2Fe_2O_5$

In thin thin, epitaxial strain can mimic anisotropic pressure effects, by creating compressed or elongated B-O distances and rotations of polyhedra.[59] Such anisotropy can be further diverged in oxygen-deficient perovskites with ordered vacancies, such as $A_2B_2O_5$ compounds, depending on the relative orientation of the vacancy order with respect to the biaxial epitaxial strain.[54] We anticipate the similar anisotropic effect by applying biaxial strain, because $Ca_2Mn_2O_5$-type structure hosts anisotropic behavior in both super-exchange and spin crossover as discussed earlier. To investigate this feature regarding magnetic order stability, we applied biaxial strain with two different orientation on $Sr_2Fe_2O_5$, as illustrated in Fig. 11(a). Orientation 1 corresponds to (001) plane of $Ca_2Mn_2O_5$-type structure, while orientation 2 is on $(\bar{2}10)$ plane. As its FM order showed monotonic decrease in relative energy with respect to AFM-G order when U is not applied, we can quantitatively estimate the pressure effect induced by each orientation.

In Fig. 11(b), stability of FM to AFM-G order is plotted with respect to pseudo-cubic lattice parameter. With orientation 1, the energy difference between FM and AFM-G order is minimized down to 400 meV/f.u., which is comparable to 5.5 GPa power of hydrostatic pressure. On the other hand, orientation 2 is able to reach less power than orientation 1, down to 462 meV/f.u.. This is only equivalent to 2 GPa of hydrostatic pressure, by having significant orientation-dependence. The first noticieable aspect in biaxial strain is that its pressure-mimicking power is much smaller than hydrostatic pressure when measured with magnetic stability of FM. This inefficiency becomes more clear when compared with the pseudocubic lattice parameter (a_{pc}). The maximum pressure effect of 5 GPa can be realized at a_{pc} of 3.75 Å with orientation 1, but the same value a_{pc} correspnds to the parameter under hydrostatic pressure of 20 GPa where the relative enthalpy of FM is 65 meV.

The reason for this inefficiency in mimicking pressure effect can be found from the relaxation of structure that elongation occurs perpendicular to biaxial plane when compressive strain is applied. For example, at 3.75 Å with orientation 1, a and b crystallographic lattices are compressed by ∼6.5%, but at the same time ∼10% of elongation along c-direction occurs so as to relax the elastic instability, while all lattice parameters decrease under hydrostatic pressure. This reaction leads to less change in unit volume that the minmum unit volume of AFM-G order is 447Å^3, which is equivalent to unit volume when ∼5 GPa of hydrostatic pressure is applied. Regarding that one of energetic motive of transitioning to FM order was with smaller unit volume, which is favorable

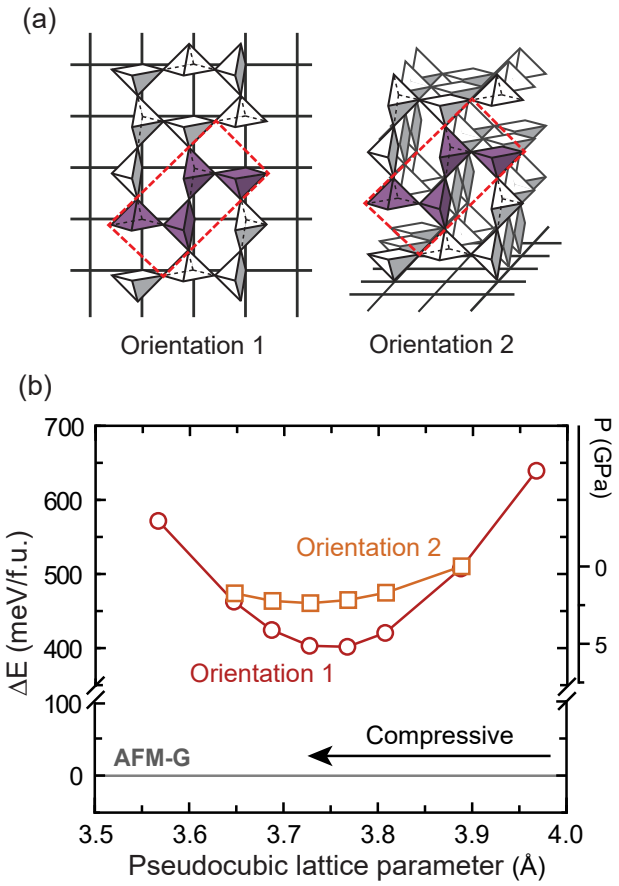

FIG. 11. (a) Schematic illustration of two biaxial orientations on $Ca_2Mn_2O_5$-type structure, with unit cell structure is highlighted with purple color and red outline. (b) Relative energy difference of FM $Sr_2Fe_2O_5$ phases compared to AFM-G phases with respect to pseudocubic lattice parameter of biaxial strain

change under hydrostatic pressure, biaxial strain weakens the motive as the out-of-plane elongation relieves the compressive condition given from biaxial strain.

The elongation along out-of-plane direction can be decomposed down to local bond length of each orientation, which explains the disparity between orientation 1 and 2. The general change of local bond length is summarized in Table V, where the basal bonds are divided into $l_{ba,ab}$ and $l_{ba,c}$ depending on bonding direction. In orientation 1, the basal bonds along c-axis ($l_{ba,c}$) are elongated while bond length along ab-plane ($l_{ba,ab}$) and apical bond length decrease. Likewise in orientation 2, the basal bond along ab-plane ($l_{ba,ab}$) increases when other bonds are reduced under compressive strain. The elongated bonds works as opposite-contributions to stabilize FM state because spin crossover is inhibitted along such elongated bonds. As each biaxial strain is with different degree of opposite contributions from stabilizing FM order, orientations exhibit different pressure-mimicking power as shown in Fig. 11(b), compared to hydrostatic pressure with cooperative contributions from all O1, O2, and O3 connections via general

decrease in all types of Fe-O bonds.

TABLE V. General change of Fe–O–Fe path length which can be decomposed to l_{ap}, $l_{ba,ab}$, and $l_{ba,c}$.

	Fe–O1–Fe		Fe–O2–Fe		Fe–O3–Fe	
Orientation	$l_{ba,c}$	$l_{ba,c}$	l_{ap}	$l_{ba,ab}$	$l_{ba,ab}$	$l_{ba,ab}$
Orientation 1	↑↑	↑↑	↓	↓↓	↓↓	↓↓
Orientation 2	↓↓	↓↓	↓	↑↑	↑↑	↑↑

The selective elongation/compression of specific type of Fe-O bonds can be used to roughly estimate the change of stability contributions from O1, O2, and O3 connections, via relative change in Fe–O–Fe path length. Each O1 connection can be composed of two Fe-O1 bonds ($l_{ba,c}$), O2 of $l_{ap} + l_{ba,ab}$, and O3 of two $l_{ba,ab}$. Thus we can estimate the change of Fe–O–Fe path length based on change in constituent increasing/decreasing bonds, which are summarized in Table V. Under compressive strain, orientation 1 experiences shortened Fe–O–Fe path length except for increasing Fe–O1–Fe path. In orientation 2, there is a competitive behavior in Fe–O2–Fe path because l_{ap} decreases while $l_{ba,ab}$ increases. Similar to the change under hydrostatic pressure, we found that l_{ap} bond is relatively insensitive to the strain and shows less change in bond length. This difference makes Fe–O2–Fe path in orientation 2 become longer as the increase in $l_{ba,ab}$ dominates the decrease in l_{ap}. As increase in Fe–O–Fe path length implies the decrease in contribution of corresponding O-connection stabilizing FM order, the orientation dependent in Fig. 11(b) is obtained.

It is noteworthy that biaxial strain induces a significant change in bond angles compared to hydrostatic pressure. In $Ca_2Mn_2O_5$-type structures, there are three types of characteristic bond angles, ∠ Fe-O1-Fe (∠O1), ∠ Fe-O2-Fe (∠O2), and ∠ Fe-O3-Fe (∠O3), where ∠O3 is set to 180° by symmetry. While hydrostatic pressure increases the ∠O1 and ∠O2 up to 10°, from 0 GPa to 30 GPa, these bond angles can be dramatically tuned depending on biaxial orientation; with orientation 1, ∠O1 increases by 17° and ∠O2 decreases by 27°, and with orientation 2, ∠O1 changes less than 1° while ∠O2 increases by XX°.

We attribute this dramatic change in bond angles as a reaction to resolve the elastic stress on (001) plane induced by stiffer apical bond under compressive condition. While basal oxygens have pair anion on the opposite direction over B cation thus subjected to compression under pressure or strain, the absence of counterpart for apical oxygen in a square pyramid makes makes B-cation displace and keeps apical bond length under compressive condition. As the compressibility of apical bond is relatively small, $Ca_2Mn_2O_5$-type structure tends to resolve the elastic instability by tuning bond angle. In orientation 1, change in bond angles makes square pyramids more like triangular bipyramids, which significantly changes the basal bonds and ∠O2 but yields more efficient packing on (001) plane. This compression on (001) plane makes the bonding along [001] direction is further elongated and ∠O1 changes toward 180°. On the other hand, orientation 2 barely experiences compression on (001) plane is perpendicular to biaxial plane and elastic instability and elastic instability can be easily resolved by relaxation along [$\bar{2}$10] direction. Thus ∠O2 rather approaches toward 180°, while only ∠O1 slightly decreases owing to compression along [001] direction whose instability is mostly resolved by change in $l_{ba,c}$.

Biaxial strain on $Sr_2Fe_2O_5$ with $Ca_2Mn_2O_5$-type structure shows that different relative orientations makes distinction in change of local bond length and bond angles. The pressure-mimicking power of biaxial strain is only equivalent to 5.5 GPa of hydrostatic pressure even under significant compressive condition, because of the relaxation along the direction perpendicular to biaxial plane while magnetic transition of $Sr_2Fe_2O_5$ require cooperative compression from whole way. Instead, the relaxation along perpendicular direction from biaxial plane introduces the significant change in local structures, which is particularly anisotropic with ordered oxygen vacancies in perovskite, and thus shows a promising strategy to stabilize unique materials phenomena sensitive to such local structures.

IV. CONCLUSION

In conclusion, we identified the nature of pressure-dependent magnetic stabilities in $Ca_2Mn_2O_5$-type oxygen-deficient perovskites, by adopting $Sr_2Mn_2O_5$ and $Sr_2Fe_2O_5$ as representative cases for d^4 and d^5 systems, respectively. We demonstrate that $Sr_2Mn_2O_5$ shows AFM-E order at ambient condition following the Goodenough-Kanamori-Anderson rule with square pyramidal crystal field splitting, where its order is further stabilized under hydrostatic pressure owing to reinforced super-exchange interaction. $Sr_2Fe_2O_5$ on the other hand shows magnetic transition from AFM-G order to FM at ∼24.5 GPa which accompanies insulator-metal transitions via spin crossover. The both behavior can be understood as hydrostatic pressure reduces the B-O bond length and reinforce the crystal field splitting. d-orbital states are broadened along energy scale, which induces different behavior in $Sr_2Mn_2O_5$ and $Sr_2Fe_2O_5$. We also investigated the effect of Hubbard U on-site potential on magnetic behavior, which yielded FM-preferable effect on $Sr_2Mn_2O_5$ but worked oppositely for d^5 systems by rather stabilizing AFM-G order. As stabilization of FM order via spin crossover is inhibited by the presence of U, higher level of pressure was required to overcome the barrier to drive magnetic transition. Lastly we evaluated the effect of biaxial strain following the measure of energy difference between FM and AFM-G order in $Sr_2Fe_2O_5$, and estimated it pressure effect is equivalent to 5.5 GPa when strain equivalent to 3.75Åpseudocubic lattice is applied on ab-crystallographic plane. The local structures with biaxial strain changes distinctly compared to structures under hydrostatic pressure, and its

dependence in relative orientation of biaxial plane can be understood based on different compressibility of B-O bonds in $Ca_2Mn_2O_5$-type structure. This study provides various benefit on magnetic materials in transition metal compounds in that the correlation between local coordination environment, polyhedral arrangement, d-orbital filling, and pressure/strain effects are comprehensively covered.

ACKNOWLEDGMENTS

Y.S. and J.M.R. acknowledge support from the the Alfred P. Sloan Foundation fellowship (FG-2016-6469). Calculations were performed using the QUEST HPC Facility at Northwestern, the Extreme Science and Engineering Discovery Environment (XSEDE), which is supported by the National Science Foundation under Grant No. ACI-1548562, and the Center for Nanoscale Materials (Carbon) Cluster, an Office of Science user facility supported by the U.S. Department of Energy, Office of Science, Office of Basic Energy Sciences, under Contract No. DE-AC02-06CH11357.

* jrondinelli@northwestern.edu

[1] E. O. Wollan and W. C. Koehler, "Neutron diffraction study of the magnetic properties of the series of perovskite-type compounds $[(1-x)\mathrm{La}, x\mathrm{Ca}]\mathrm{Mno}_3$," Phys. Rev. **100**, 545–563 (1955).

[2] J. Hemberger, A. Krimmel, T. Kurz, H.-A. Krug von Nidda, V. Yu. Ivanov, A. A. Mukhin, A. M. Balbashov, and A. Loidl, "Structural, magnetic, and electrical properties of single-crystalline $\mathrm{la}_{1-x}\mathrm{sr}_x\mathrm{mno}_3$ $(0.4 < x < 0.85)$," Phys. Rev. B **66**, 094410 (2002).

[3] V. Caignaert, "$\mathrm{Sr}_2\mathrm{mn}_2\mathrm{o}_5$ magnetic structure," Journal of Magnetism and Magnetic Materials **166**, 117 – 123 (1997).

[4] Nianpeng Lu, Pengfei Zhang, Qinghua Zhang, Ruimin Qiao, Qing He, Hao-Bo Li, Yujia Wang, Jingwen Guo, Ding Zhang, Zheng Duan, Zhuolu Li, Meng Wang, Shuzhen Yang, Mingzhe Yan, Elke Arenholz, Shuyun Zhou, Wanli Yang, Lin Gu, Ce-Wen Nan, Jian Wu, Yoshinori Tokura, and Pu Yu, "Electric-field control of tri-state phase transformation with a selective dual-ion switch," Nature **546**, 124–128 (2017), letter.

[5] Josie E. Auckett, Andrew J. Studer, Neeraj Sharma, and Chris D. Ling, "Floating-zone growth of brownmillerite $\mathrm{sr}_2\mathrm{fe}_2\mathrm{o}_5$ and the observation of a chain-ordered superstructure by single-crystal neutron diffraction," Solid State Ionics **225**, 432–436 (2012).

[6] Josie E. Auckett, Andrew J. Studer, Eric Pellegrini, Jacques Ollivier, Mark R. Johnson, Helmut Schober, Wojciech Miiller, and Chris D. Ling, "Combined experimental and computational study of oxide ion conduction dynamics in $\mathrm{sr}_2\mathrm{fe}_2\mathrm{o}_5$ brownmillerite," Chemistry of Materials **25**, 3080–3087 (2013).

[7] Hannes Krger and Volker Kahlenberg, "Incommensurately modulated ordering of tetrahedral chains in ca2fe2o5at elevated temperatures," Acta Crystallographica Section B Structural Science **61**, 656–662 (2005).

[8] Thomas G. Parsons, Hans D'Hondt, Joke Hadermann, and Michael a. Hayward, "Synthesis and Structural Characterization of $\mathrm{La}_{1-x}A_x\mathrm{MnO}_{2.5}$($A$ = Ba, Sr, Ca) Phases: Mapping the Variants of the Brownmillerite Structure," Chemistry of Materials **21**, 5527–5538 (2009).

[9] K.R. Poeppelmeier, M.E. Leonowicz, J.C. Scanlon, J.M. Longo, and W.B. Yelon, "Structure determination of camno_3 and $\mathrm{camno}_{2.5}$ by x-ray and neutron methods," Journal of Solid State Chemistry **45**, 71 – 79 (1982).

[10] K.R. Poeppelmeier, M.E. Leonowicz, and J.M. Longo, "$\mathrm{Camno}_{2.5}$ and $\mathrm{ca}_2\mathrm{mno}_{3.5}$: New oxygen-defect perovskite-type oxides," Journal of Solid State Chemistry **44**, 89 – 98 (1982).

[11] V. Caignaert, N. Nguyen, M. Hervieu, and B. Raveau, "$\mathrm{Sr}_2\mathrm{mn}_2\mathrm{o}_5$, an oxygen-defect perovskite with mn(iii) in square pyramidal coordination," Materials Research Bulletin **20**, 479 – 484 (1985).

[12] Feng Zhu, Ye Wu, Xiaojing Lai, Shan Qin, Ke Yang, Jing Liu, and Xiang Wu, "Experimental and theoretical investigations on high-pressure phase transition of $\mathrm{sr}_2\mathrm{fe}_2\mathrm{o}_5$," Physics and Chemistry of Minerals **41**, 449–459 (2014).

[13] JB Goodenough, "In magnetism and the chemical bond; cotton, fa; olah, ga; prigogine, i., eds.; interscience monographs chemistry," (1963).

[14] Junjiro Kanamori, "Superexchange interaction and symmetry properties of electron orbitals," Journal of Physics and Chemistry of Solids **10**, 87 – 98 (1959).

[15] P. W. Anderson, "New approach to the theory of superexchange interactions," Phys. Rev. **115**, 2–13 (1959).

[16] G. Kresse and J. Furthmüller, "Efficient iterative schemes for *ab initio* total-energy calculations using a plane-wave basis set," Phys. Rev. B **54**, 11169–11186 (1996).

[17] G. Kresse and D. Joubert, "From ultrasoft pseudopotentials to the projector augmented-wave method," Phys. Rev. B **59**, 1758–1775 (1999).

[18] John P. Perdew, Kieron Burke, and Matthias Ernzerhof, "Generalized gradient approximation made simple," Phys. Rev. Lett. **77**, 3865–3868 (1996).

[19] S. L. Dudarev, G. A. Botton, S. Y. Savrasov, C. J. Humphreys, and A. P. Sutton, "Electron-energy-loss spectra and the structural stability of nickel oxide: An lsda+u study," Phys. Rev. B **57**, 1505–1509 (1998).

[20] P. E. Blöchl, "Projector augmented-wave method," Phys. Rev. B **50**, 17953–17979 (1994).

[21] Hendrik J. Monkhorst and James D. Pack, "Special points for brillouin-zone integrations," Phys. Rev. B **13**, 5188–5192 (1976).

[22] Peter E. Blöchl, O. Jepsen, and O. K. Andersen, "Improved tetrahedron method for brillouin-zone integrations," Phys. Rev. B **49**, 16223–16233 (1994).

[23] A. I. Liechtenstein, V. I. Anisimov, and J. Zaanen, "Density-functional theory and strong interactions: Orbital ordering in mott-hubbard insulators," Phys. Rev. B **52**, R5467–R5470 (1995).

[24] P. Adler, U. Schwarz, K. Syassen, A.P. Milner, M.P. Pasternak, and M. Hanfland, "Structural phase transitions in sr$_2$fe$_2$o$_5$ under high pressure," Journal of Solid State Chemistry **155**, 381 – 388 (2000).

[25] There are several nomenclatures used for AFM-E order: G_xA_y,[3] A_y[30] (noting that the $Sr_2Mn_2O_5$ is without non-collinear nature), and D-type AFM.[60] In this study we adopt E-type AFM focusing on the similarity with AFM-E order[61]? which follows Wollan-Koehler standard notation .

[26] S. Picozzi, K. Yamauchi, G. Bihlmayer, and S. Blügel, "First-principles stabilization of an unconventional collinear magnetic ordering in distorted manganites," Phys. Rev. B **74**, 094402 (2006).

[27] J. Laverdière, S. Jandl, A. A. Mukhin, V. Yu. Ivanov, V. G. Ivanov, and M. N. Iliev, "Spin-phonon coupling in orthorhombic rMno$_3$ (r = Pr, Nd, Sm, Eu, Gd, Tb, Dy, Ho, Y): A raman study," Phys. Rev. B **73**, 214301 (2006).

[28] T. C. Han and H. H. Chao, "Observation of large electric polarization in orthorhombic tmmno3 thin films," Applied Physics Letters **97**, 232902 (2010), https://doi.org/10.1063/1.3524500.

[29] Bernd Lorenz, Ya-Qi Wang, and Ching-Wu Chu, "Ferroelectricity in perovskite HoMno$_3$ and YMno$_3$," Phys. Rev. B **76**, 104405 (2007).

[30] Leopoldo Suescun, Omar Chmaissem, James Mais, Bogdan Dabrowski, and James D. Jorgensen, "Crystal structures, charge and oxygen-vacancy ordering in oxygen deficient perovskites srmnox (x<2.7)," Journal of Solid State Chemistry **180**, 1698 – 1707 (2007).

[31] Leopoldo Suescun, Bogdan Dabrowski, James Mais, Steven Remsen, James W. Richardson, Evan R. Maxey, and James D. Jorgensen, "Oxygen ordered phases in la$_x$sr$_{1x}$mno$_y$($0 \le x \le 0.2$, $2.5 \le y \le 3$): An in situ neutron powder diffraction study," Chemistry of Materials **20**, 1636–1645 (2008), https://doi.org/10.1021/cm703139c.

[32] Exclusively for $La_2Mn_2O_5$ the Hubbard U of 3 eV was applied to Mn as we observed significant delocalization of electrons, which is similar to incorrect description of electronic/magnetic structures in $LaMnO_3$ with absence of U.?? We note that other the shape of energy landscape was nearly intact regardless of U in $Sr_2Mn_2O_5$ and $Sr_2Fe_2O_5$.

[33] M. Marezio and P.D. Dernier, "The bond lengths in lafeo3," Materials Research Bulletin **6**, 23 – 29 (1971).

[34] M.J. Sayagus, J.M. Crdoba, and F.J. Gotor, "Room temperature mechanosynthesis of the la1xsrxmno3 (0x1) system and microstructural study," Journal of Solid State Chemistry **188**, 11 – 16 (2012).

[35] The coupling constants in this work are calculated by applying different magnetic orders on structures of the most stable magnetic order at each pressure. We induced antiferromagnetic or ferromagnetic interaction on each type of bridging oxygens, which yields 8 different magnetic orders from 3 types of oxygen sites (2^3=8).

[36] J.-S. Zhou, J. A. Alonso, A. Muoñz, M. T. Fernández-Díaz, and J. B. Goodenough, "Magnetic structure of lacro$_3$ perovskite under high pressure from in situ neutron diffraction," Phys. Rev. Lett. **106**, 057201 (2011).

[37] G. A. Samara and A. A. Giardini, "Effect of pressure on the néel temperature of magnetite," Phys. Rev. **186**, 577–580 (1969).

[38] J.-S. Zhou and J. B. Goodenough, "Unusual evolution of the magnetic interactions versus structural distortions in $r$mno$_3$ perovskites," Phys. Rev. Lett. **96**, 247202 (2006).

[39] Yang Ding, Daniel Haskel, Yuan-Chieh Tseng, Eiji Kaneshita, Michel van Veenendaal, J. F. Mitchell, Stanislav V. Sinogeikin, Vitali Prakapenka, and Ho-kwang Mao, "Pressure-induced magnetic transition in manganite (la$_{0.75}$ca$_{0.25}$mno$_3$)," Phys. Rev. Lett. **102**, 237201 (2009).

[40] A Sacchetti, P Postorino, and M Capone, "High-pressure phase diagram in the manganites: a two-site model study," New Journal of Physics **8**, 3 (2006).

[41] L. Pinsard-Gaudart, J. Rodríguez-Carvajal, A. Daoud-Aladine, I. Goncharenko, M. Medarde, R. I. Smith, and A. Revcolevschi, "Stability of the jahn-teller effect and magnetic study of lamno$_3$ under pressure," Phys. Rev. B **64**, 064426 (2001).

[42] I. Loa, P. Adler, A. Grzechnik, K. Syassen, U. Schwarz, M. Hanfland, G. Kh. Rozenberg, P. Gorodetsky, and M. P. Pasternak, "Pressure-induced quenching of the jahn-teller distortion and insulator-to-metal transition in lamno$_3$," Phys. Rev. Lett. **87**, 125501 (2001).

[43] M. Baldini, V. V. Struzhkin, A. F. Goncharov, P. Postorino, and W. L. Mao, "Persistence of jahn-teller distortion up to the insulator to metal transition in lamno$_3$," Phys. Rev. Lett. **106**, 066402 (2011).

[44] R Qiu, E Bousquet, and A Cano, "Pressure-induced insulatormetal transition in $EuMnO_3$," Journal of Physics: Condensed Matter **29**, 305801 (2017).

[45] Jun-Shuai Chai, Hao Tian, Ai-Jie Mao, Li-Juan Deng, and Xiao-Yu Kuang, "Pressure effect on the properties of magnetic moments and phase transitions in ymno3 from first principles," RSC Adv. **6**, 54041–54048 (2016).

[46] Shintaro Ishiwata, Yoshio Kaneko, Yusuke Tokunaga, Yasujiro Taguchi, Taka-hisa Arima, and Yoshinori Tokura, "Perovskite manganites hosting versatile multiferroic phases with symmetric and antisymmetric exchange strictions," Phys. Rev. B **81**, 100411 (2010).

[47] Shintaro Ishiwata, Yusuke Tokunaga, Yasujiro Taguchi, and Yoshinori Tokura, "High-pressure hydrothermal crystal growth and multiferroic properties of a perovskite ymno3," Journal of the American Chemical Society **133**, 13818–13820 (2011), https://doi.org/10.1021/ja205408m.

[48] R. D. Shannon, "Revised effective ionic radii and systematic studies of interatomic distances in halides and chalcogenides," Acta Crystallographica Section A **32**, 751–767 (1976).

[49] If higher level of pressure is applied, we anticipate that spin crossover in d^4 system can also occur. Though up-spin $d_{x^2-y^2}$ states goes up in the energy by pressure, higher pressure will eventually broaden spin-down d-states so that it crosses the fermi level at some point. Indeed, a first-principles study reported spin crossover of Mn^{3+} between 40 and 50 GPa.[45] Based on our preliminary calculation, we observe no spin crossover up to 60 GPa in $Ca_2Mn_2O_5$-type structure.

[50] Takateru Kawakami and Hiroshi Kageyama, "High-spin to intermediate-spin transition, insulator-metal transition, and antiferro- to ferromagnetic transition in srfeo$_2$ under high pressure," Zeitschrift fr Kristallographie **225** (2010), 10.1524/zkri.2010.1311.

[51] T. Kawakami, Y. Tsujimoto, H. Kageyama, Xing-Qiu Chen, C. L. Fu, C. Tassel, A. Kitada, S. Suto, K. Hirama, Y. Sekiya, Y. Makino, T. Okada, T. Yagi, N. Hayashi, K. Yoshimura, S. Nasu, R. Podloucky, and M. Takano, "Spin transition in a four-coordinate iron oxide," Nature Chemistry **1**, 371–376 (2009).

[52] M. Takano, S. Nasu, T. Abe, K. Yamamoto, S. Endo, Y. Takeda, and J. B. Goodenough, "Pressure-induced high-spin to low-spin transition in cafeo$_3$," Phys. Rev. Lett. **67**, 3267–3270 (1991).

[53] O. E. González-Vázquez and Jorge Íñiguez, "Pressure-induced structural, electronic, and magnetic effects in bifeo$_3$," Phys. Rev. B **79**, 064102 (2009).

[54] Joshua Young and James M. Rondinelli, "Crystal structure and electronic properties of bulk and thin film brownmillerite oxides," Phys. Rev. B **92**, 174111 (2015).

[55] Chunlan Ma, Zhongqin Yang, and Silvia Picozzi, "Ab initio electronic and magnetic structure in la 0.66 sr 0.33 mno 3 : strain and correlation effects," Journal of Physics: Condensed Matter **18**, 7717 (2006).

[56] R Rozilah, M K Yaakob, Z Mohamed, and A K Yahya, "Effects of on-site coulomb interaction (u) on the structural and electronic properties of half-metallic ferromagnetic orthorhombic $pr_{0.75}na_{0.25}mno_3$ manganite: a lda+ u calculation and experimental study," Materials Research Express **4**, 066103 (2017).

[57] Igor Solovyev, Noriaki Hamada, and Kiyoyuki Terakura, "t_{2g} versus all 3d localization in lamo$_3$ perovskites (m=ti–cu): First-principles study," Phys. Rev. B **53**, 7158–7170 (1996).

[58] O. E. González-Vázquez and Jorge Íñiguez, "Pressure-induced structural, electronic, and magnetic effects in bifeo$_3$," Phys. Rev. B **79**, 064102 (2009).

[59] Darrell G. Schlom, Long-Qing Chen, Chang-Beom Eom, Karin M. Rabe, Stephen K. Streiffer, and Jean-Marc Triscone, "Strain tuning of ferroelectric thin films," Annual Review of Materials Research **37**, 589–626 (2007), https://doi.org/10.1146/annurev.matsci.37.061206.113016.

[60] Pan Liu, Wei-Hua Wang, Wei-Chao Wang, Ya-Hui Cheng, Feng Lu, and Hui Liu, "D-type anti-ferromagnetic ground state in ca 2 mn 2 o 5," Chinese Physics Letters **34**, 027101 (2017).

[61] Chung-Yuan Ren, "Atomic, electronic, and ferroelectric properties of manganite $r$mno$_3$ (r = Ho, Er, Tm, Lu) in hexagonal and orthorhombic phases," Phys. Rev. B **79**, 125113 (2009).